Intermetallics 126 (2020) 106942

Contents lists available at ScienceDirect

Intermetallics

journal homepage: http://www.elsevier.com/locate/intermet

Effect of irradiation on randomness of element distribution in CoCrFeMnNi equiatomic high-entropy alloy

X.L. Ren [a,b], B.D. Yao [c], T. Zhu [a,d], Z.H. Zhong [e], Y.X. Wang [b], X.Z. Cao [d], S. Jinno [f], Q. Xu [a,*]

[a] Institute for Integrated Radiation and Nuclear Science, Kyoto University, Osaka, 590-0494, Japan
[b] Key Laboratory of Nuclear Physics and Ion-beam Application (MOE), Institute of Modern Physics, Department of Nuclear Science and Technology, Fudan University, Shanghai, 200433, China
[c] Shandong Peninsula Engineering Research Center of Comprehensive Brine Utilization, Weifang University of Science and Technology, Shandong, 262700, China
[d] Institute of High Energy Physics, Chinese Academy of Sciences, Beijing, 100049, China
[e] School of Materials Science and Engineering, Hefei University of Technology, Hefei, 230031, China
[f] Nuclear Professional School, School of Engineering, The University of Tokyo, Ibaraki, 319-1188, Japan

ARTICLE INFO

Keywords:
High-entropy alloy
Ab initio calculations
Element distribution
Ion irradiation

ABSTRACT

The stability of the structure and composition of the alloy is important in structural materials. Therefore, in this study, the distribution of each element in the CoCrFeMnNi equiatomic high-entropy alloy (HEA), which is considered to have a random distribution, was examined experimentally and theoretically. Furthermore, the effect of ion irradiation at different temperatures on the distribution of each element was investigated. The experimental results based on the positron annihilation spectroscopy showed that there was not significant element segregation in the well-annealed CoCrFeMnNi HEA. Moreover, the distribution of the elements in CoCrFeMnNi HEA was approximately the same despite the alloy being irradiated to 0.5 dpa (displacement per atom) at the damage peak at temperatures of 300, 573, and 773 K. In addition, the randomness of the element distribution in the equilibrium structure of the CoCrFeMnNi HEA was investigated using the first-principles simulation. The calculation results showed that despite the favorable affinity between Ni and Cr in the CoCrFeMnNi HEA, the constituent elements in the alloy were disordered. In addition, the same-type atomic pairings of an element with itself, especially Cr-Cr, were all depleted.

1. Introduction

In recent years, studies on high-entropy alloys (HEAs), which are defined as alloys that show single solid solution phases and are made by mixing five or more elements with an approximately equiatomic composition ratio [1–3], which have been actively conducted globally to enhance metallic materials [4–6]. Some HEAs have excellent high-temperature strengths, favorable ductility, and outstanding low-temperature fracture toughness. Therefore, research on HEAs has drawn attention for its practical uses. The face-centered cubic (FCC) single-phase solid solution CoCrFeMnNi equiatomic composition ratio alloy, which was first reported by Cantor et al. [7], is the most studied. The excellent mechanical properties of the CoCrFeMnNi high-entropy alloy (HEA) are well known [8–10].

The CoCrFeMnNi HEA showed a high swelling resistance under high temperature and high dose of Ni ion irradiation [11]. Specifically, this alloy contains elements, such as Co and Ni, that can produce a highly radioactive substance caused by a nuclear reaction with neutrons. Therefore, the CoCrFeMnNi HEA cannot be used as a nuclear material. However, if the mechanism of the irradiation resistance of the CoCrFeMnNi HEA is known, low-activation high-entropy alloys can be developed based on this mechanism. Generally, the structural and compositional stability of structural materials are major factors in maintaining excellent performance. The introduction of point defects using irradiation with high-energy particles or cold working increases the rate of diffusion of atoms in the material, which may change the composition of the material. For example, it was reported that vacancies formed in an Fe-based FeCrMnCuMo multi-component alloy using irradiation at low temperature promoted the formation of Cu precipitate during annealing at high temperatures [12]. It was also reported that Cr-rich precipitates were formed in plastic-deformed CoCrFeMnNi HEA following prolonged exposure at high temperatures [13,14]. In addition,

* Corresponding author.
E-mail address: xu.qiu.8z@kyoto-u.ac.jp (Q. Xu).

https://doi.org/10.1016/j.intermet.2020.106942
Received 1 July 2020; Received in revised form 3 August 2020; Accepted 16 August 2020
Available online 24 August 2020

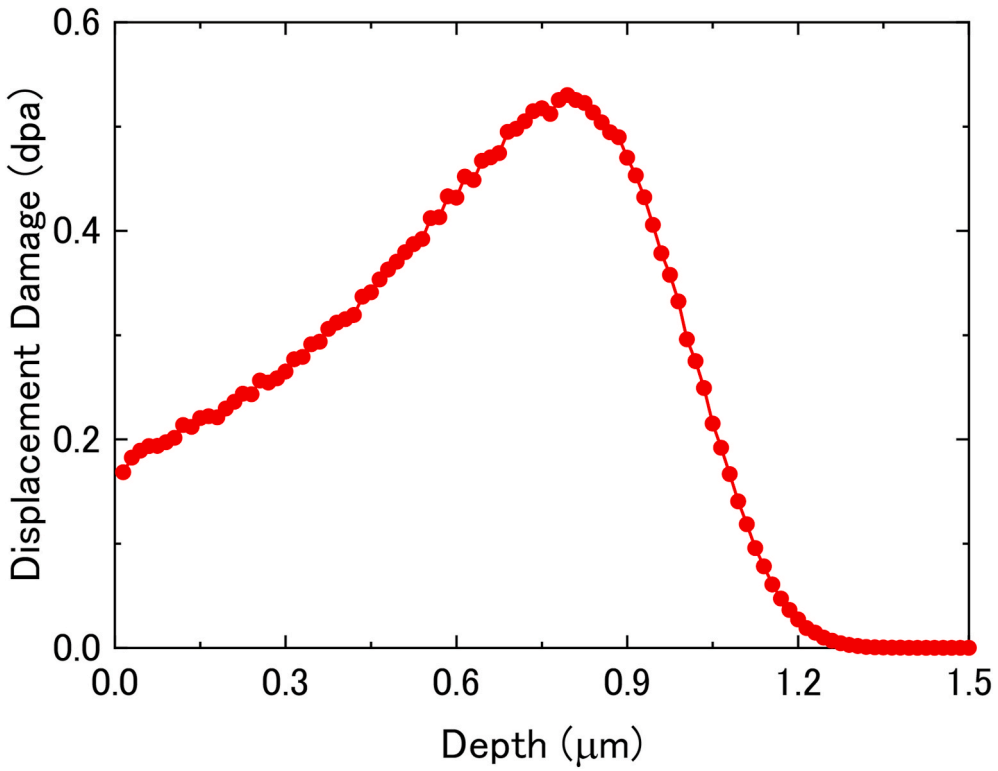

Fig. 1. Simulation of the damage distribution in the CrCoFeMnNi HEA irradiated by 2.8 MeV Fe ions up to 5×10^{18} ions/m^2 using the SRIM code.

in FeCr binary alloy, the segregation of elements occurs due to irradiation or long-term aging at high temperatures.

In this study, the distribution of the elements in the well-annealed CoCrFeMnNi HEA was investigated using experiments and calculations based on the first-principles. In addition, the effects of ion irradiation on the element distribution in the same alloy were also investigated.

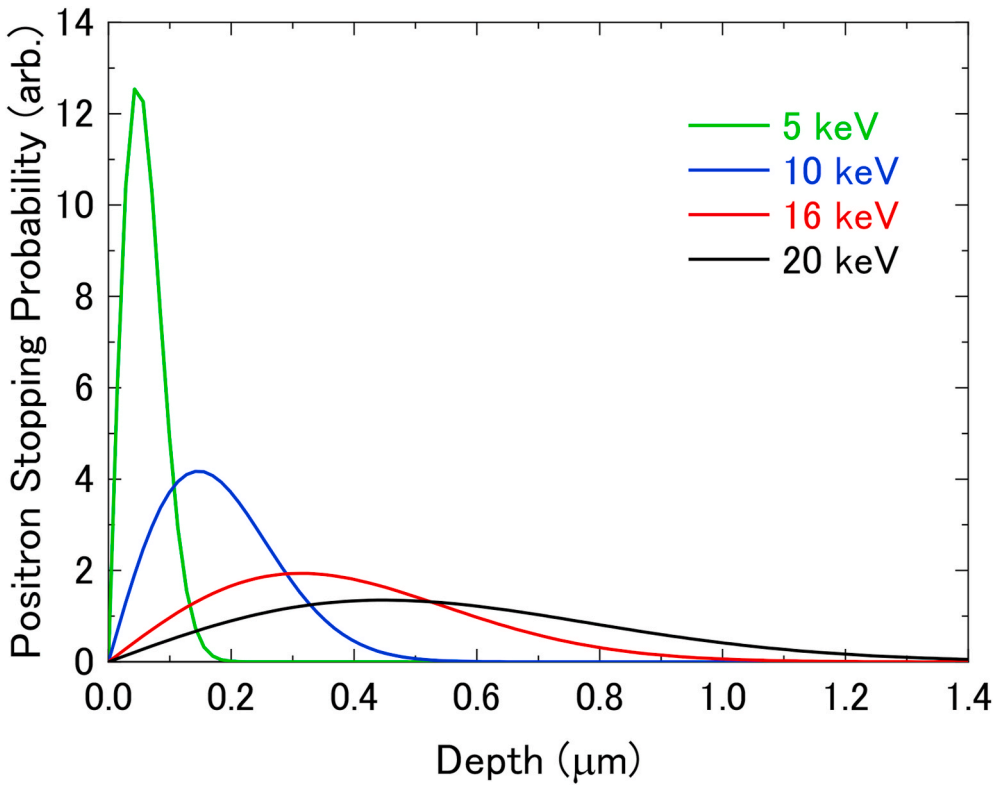

Fig. 2. Depth profile positron stopping probability for the positron energies of 5, 10, 16, and 20 keV in the CrCoFeMnNi HEA.

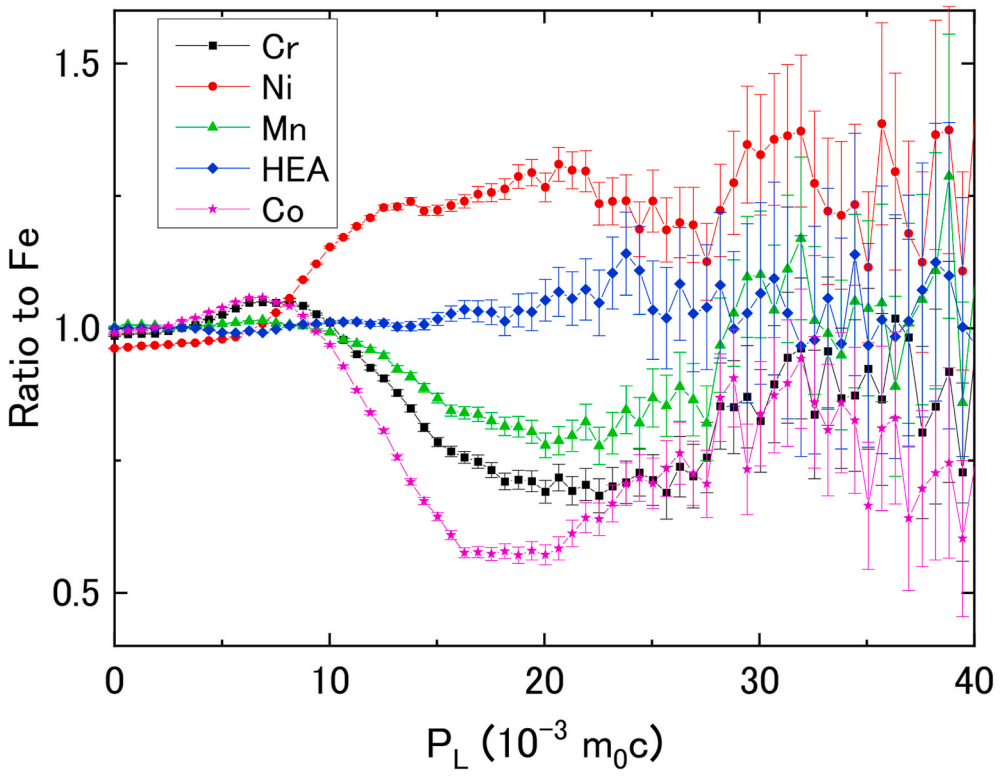

Fig. 3. CDB ratio curves of CrCoFeMnNi HEA, Cr, Co, Mn, and Ni to pure Fe.

2. Experimental and computational methods

2.1. Experimental procedure

The CoCrFeMnNi HEA (20 at.%, nominal composition) was melted in a MgO crucible in a vacuum induction furnace with high-purity (>99%) elements of Co, Cr, Fe, Mn, and Ni. It was then homogenized in a vacuum at 1473 K for 10 h. Square specimens (10 mm × 10 mm) with thicknesses of 0.2 mm were cut out from the ingot using electrical discharge machining. The surfaces of the samples were mechanically polished to a mirror surface and annealed in a high vacuum (~10^{-5} Pa) at 1273 K for 1 h to eliminate defects introduced during cutting and polishing. To investigate the effect of irradiation on the compositional stability of the CoCrFeMnNi HEA, 2.8 MeV Fe ion irradiation was conducted using a tandem type accelerator. The irradiation temperatures were 300, 573, and 773 K, and the ion fluence was 5 × 10^{18} ions/m^2. Fig. 1 shows the depth distribution of damage in the CoCrFeMnNi HEA after the ion irradiation. The damage peak was 800 nm from the surface, and the damage was 0.5 dpa (displacements per atom).

Positron annihilation spectroscopy (PAS) was used to investigate the segregation of the elements in the CoCrFeMnNi HEA before and after the ion irradiation. The annihilation partners of the positrons in the metals were the valence and core electrons. The former has little on the 0.511 MeV energy of gamma rays emitted after annihilation with positrons, but the latter has momentum energy, which affects the gamma ray energy through the Doppler effect (Doppler broadening). As a result, the element can be identified by measuring the momentum distribution of the core electrons. As described above, the depth of the damaged region of the CoCrFeMnNi HEA irradiated with 2.8 MeV Fe ions is approximately 1 μm. In order to measure the compositional change in this region, it was impossible to use PAS based on the ordinary positron source method using a measurement region of approximately 0.1 mm. Therefore, the ion-irradiated samples were measured using a mono-energetic positron beam capable of adjusting the measurement depth, which was installed at the Institute of High Energy Physics of the Chinese Academy of Sciences. Fig. 2 shows the depth profile of the positron stopping probability for the positron energies of 5, 10, 16, and 20 keV in the CoCrFeMnNi HEA, which was calculated using the following equation [15,16]:

$$P(x,E) = -\frac{d}{dx}\exp\left(-x^m / x_0^m\right) \quad (1)$$

where, $x_0 = (\alpha/\rho)E^n$, ρ is the material density, which was 8.068 g/cm^3 in this study; E (keV) is the incident positron energy; and x (cm) is the distance from the surface. In addition, we used the following Makhovian parameters: α = 4.0 μg/cm^2/$keV^{-1.6}$, m = 2, and n = 1.62, which were determined by Vehanen et al. [16]. Because the 16 keV positron depth profile approximately covered the damage due to the 2.8 MeV Fe ions in the CoCrFeMnNi HEA, Coincidence Doppler broadening (CDB) measurements were conducted using 16 keV positrons. The low- and high-momentum regions in the CDB spectra were due to the annihilation of positrons with valence and core electrons, respectively. Therefore, the former and latter can obtain information on vacancies and vacancy clusters, and segregation of elements and precipitation, respectively.

2.2. Computational method

A combination of the Metropolis Monte Carlo (MMC) and density functional theory (DFT) method was used to search for the equilibrium structure of the CoCrFeMnNi HEA. The MMC method was used to obtain the global energy minimization with a Markov chain. Meanwhile, the DFT calculations of the structure energy provided a comprehensive evaluation of the structural stability. The algorithm starts with a disordered lattice structure. A pair of atoms was randomly chosen and exchanged to create a new configuration. The structural energies of the new and old configurations were calculated using the DFT method. The acceptance possibility of a new configuration was decided based on the MMC method. The details of the hybrid MMC/DFT method can be found elsewhere [17].

The first-principle calculations based on the DFT were performed

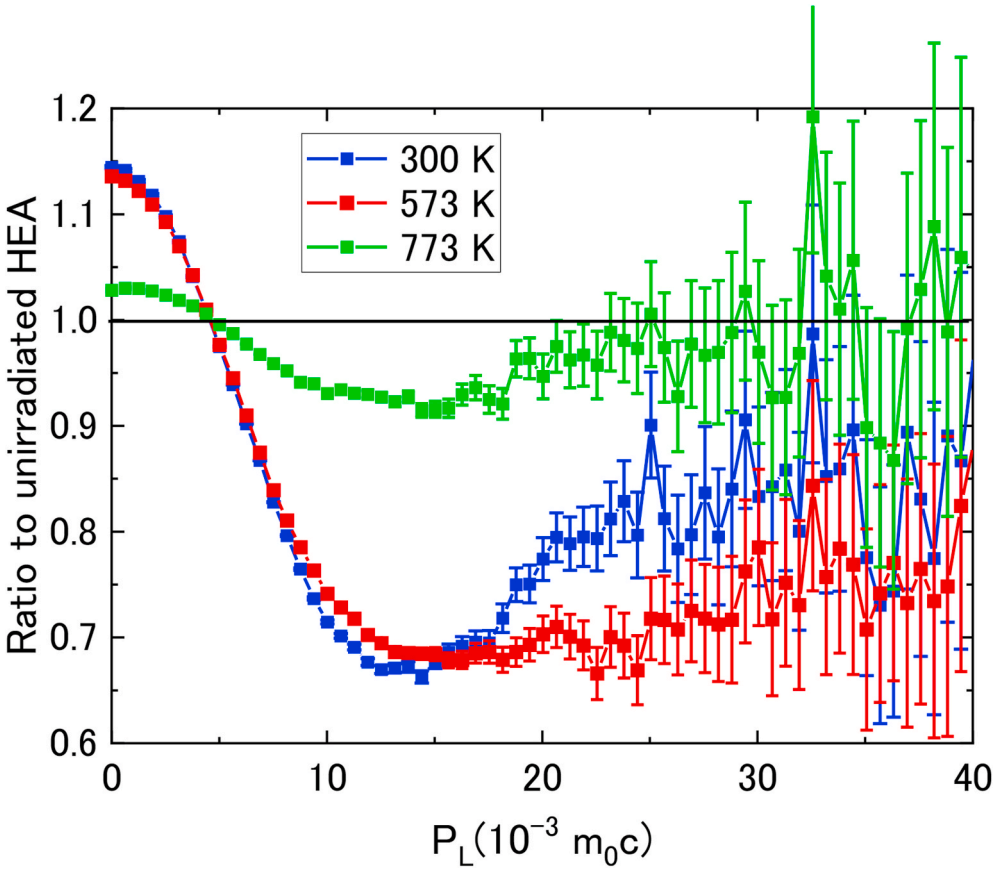

Fig. 4. CDB ratio curves of the irradiated CrCoFeMnNi HEA at 300, 573, and 773 K to the unirradiated CrCoFeMnNi HEA.

using the Vienna ab initio simulation package (VASP). The exchange correlation functionals were selected as generalized gradient approximations (GGA) determined using Perdew-Burke-Ernzerhof (PBE). A supercell containing 125 atoms was selected for the simulations. Two computational accuracies were adopted in the DFT calculations. In the hybrid MMC/DFT simulations, the search for the equilibrium state requires thousands of MMC steps, which corresponds to a high computational cost. Instead, lower-fidelity DFT calculations use an energy cutoff of 330eV and Γ-centered K-point mesh. The energy convergence and force convergence criterion were 0.1 meV and 20 meV/Å, respectively. The configuration was fully relaxed before and after the atom exchange. When the equilibrium configuration was obtained, we further optimized the configuration using a more accurate computational setting: an energy cutoff of 350eV and a 3 × 3 × 3 K-points. The energy convergence was obtained as 0.01 meV and the force convergence criterion was 10 meV/Å. The spin-polarized scheme was considered in all calculations.

The random configurations were built using the SQS code in the alloy theoretic automated toolkit (ATAT) package. The pair correlation functions up to the third neighbor shell are considered in the optimization of the SQS. The SRO parameters defined by Cowley et al. [18] was used to quantify the chemical ordering of the HEA. The SRO was calculated as: $\alpha_{ij}^n = 1 - p_{ij}^n/x_j$, where p_{ij}^n is the probability of finding an atom of j type around an atom of i type in the n-th neighboring shell and x_j is the atomic proportion of type j. $\alpha_{ij} = 0$ corresponds to a random state of the i-j atom pair. The $\alpha_{ij} > 0$ or $\alpha < 0$ correspond to the poor and rich of i-j atom pairs, respectively.

A parameter originating from the fixed metallic radii can be used to measure the atomic size difference in HEAs [19],

$$\delta = \sqrt{\sum_{i=1}^{n} c_i(1 - r_i/\bar{r})} \quad (2)$$

where n is the number of components of HEAs, $\bar{r}$ is the average radius of all the atoms; c_i and r_i are the atomic concentration and radius of the i-th element, respectively. The Wigner-Seitz (WS) radius of pure metals can be estimated using $r_{WS} = \sqrt[3]{3a^3/4\pi N}$, where N and a are the number of atoms and lattice constant in the lattice cell, respectively.

3. Results and discussion

3.1. Element distribution in the well-annealed CoCrFeMnNi HEA

Fig. 3 illustrates the CDB ratio curve of the well-annealed CoCrFeMnNi HEA to the well-annealed pure Fe. When the CDB ratio curve is parallel to the straight line y = 1, it indicates the segregation of Fe in CoCrFeMnNi HEA. For comparison, the ratio curves of the other elements such as Co, Cr, Ni, and Mn were also shown in the same figure. There was a peak in the ratio curve of the CoCrFeMnNi HEA on the horizontal axis approximately $2.5 \times 10^{-2}\ m_0c$, where m_0 is the electron rest mass, and c is the velocity of light. On the other hand, the Ni ratio curve exhibited a peak at approximately $2.0 \times 10^{-2}\ m_0c$, and other elements Co, Cr, and Mn had no peak, and there was a valley at approximately 1.7×10^{-2}, 2.1×10^{-2}, $2.1 \times 10^{-2}\ m_0c$, respectively. Thus, the ratio curve of the CoCrFeMnNi HEA did not overlap with the peaks or valleys of elemental Ni, Co, Cr, and Mn. Therefore, it was considered that element segregation did not occur, and the peak appearing at $2.5 \times 10^{-2}\ m_0c$ was unique to the CoCrFeMnNi HEA.

3.2. Effect of ion irradiation on the distribution of elements in the CoCrFeMnNi HEA

Fig. 4 shows the CDB ratio curves of the ion-irradiated to unirradiated CoCrFeMnNi HEA, where the irradiation temperatures were 300,

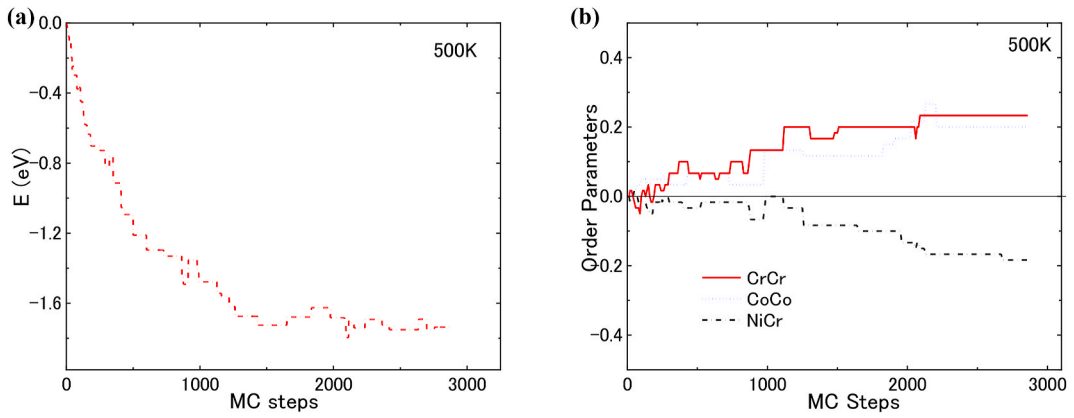

Fig. 5. System evolution of the hybrid MMC/DFT simulation at 500 K. (a) Structural cohesive energy; (b) Structural SRO parameters.

573, and 773 K. The straight line y = 1 represents the unirradiated sample. After the ion irradiation, the values of the ratio curves were larger than 1 in the low-momentum region ($P_L < 4 \times 10^{-3}\ m_0c$). In particular, the values of the samples irradiated at 300 and 573 K were higher than those irradiated at 773 K. As mentioned above, values higher than 1 in the low-momentum region meant that the vacancy clusters were formed using ion irradiation. Generally, the formation of vacancy clusters depends on the vacancy concentration and the thermal stability of the vacancy clusters. The vacancy concentration is determined by the temperature-dependent diffusion of vacancies and the concentration of sinks, such as grain boundaries. As the temperature increases, the rate of vacancy diffusion increases, and the number of vacancies eliminated at the sinks increases. As a result, the vacancy concentration decreases. On the other hand, the vacancy clusters grow easily due to the faster rate of diffusion. In some cases, the total number of vacancies that contribute to the value of the ratio curves in the low-momentum region may not decrease as much as expected relative to the increase in temperature. Therefore, it is considered that the cause of the rapid decrease in the value of the ratio curves in the low-momentum region at 773 K is the low thermal stability of vacancy clusters. Moreover, the ratio curve of the irradiation at 773 K was closer to the y = 1 line than the other irradiations. This indicated that despite the irradiation dose being the same, there were fewer defects remained at 773 K. Elsayed et al. reported the existence of tiny vacancy clusters (probably di-vacancy clusters) in CoCrFeMnNi HEA made by spark plasma sintering, and these clusters recovered with increasing temperature during isochronal annealing. The recovery was nearly complete at 600 K [20], meaning it was difficult to have tiny vacancy clusters at temperatures over 600 K. This is consistent with the results of the present study. In addition, no significant peaks were observed in the high-momentum region of the ratio curves. This indicates that there was no segregation due to irradiation in the high-entropy alloy.

3.3. Analysis of element distribution in the CoCrFeMnNi HEA based on first-principles calculations

Based on the results of the CDB experiment, it was found that the well-annealed CoCrFeMnNi HEA did not exhibit significant element segregation. It was reported that the detection of Cu precipitates in Fe using CDB requires the size of Cu precipitates be at least 0.6 nm [21], which is large enough for approximately 13 Cu atoms. This means the CDB method cannot measure the Cu segregation in smaller clusters with fewer atoms. Similarly, the CDB method is considered to be difficult for the segregation of elements for several atoms in the CoCrFeMnNi HEA. Here, the local element distribution was investigated based on first-principles calculations to further analyze the detailed ordering in the CoCrFeMnNi HEA.

The hybrid MMC/DFT simulations started from the SQS structure and were performed at 500 and 1200 K. As shown in Fig. 5, the evolution of the structural cohesive energy (Fig. 5 (a)) and structural SRO parameter (Fig. 5 (b)) was monitored. At 500K, when the simulation was approximately 3000 MC steps, the change in energy from the atom exchange was in the order of 1 meV/atom. We hypothesized that the equilibrium state was achieved. Meanwhile, the SRO parameters tend to be steady at the equilibrium stage. The obtained final SRO structure and initial SQS structure was fully relaxed for further comparison and analysis as shown in Table 1. The SRO structure was more compact and

Table 1
Calculated properties for the short range order (SRO) structure and special quasirandom structure (SQS) of the CoCrFeMnNi HEA: lattice constants, total energy per atom, and structural volume per atom.

Structure	Lattice constant (Å)	Total energy (eV)	Volume (Å^3)
SRO	3.537	−7.831	11.17
SQS	3.556	−7.790	11.01
Expt [22].	3.585		

Table 2
Mixing enthalpy (KJ/mol) of the binary systems containing the elements in CrCoFeMnNi HEA [24].

Mixing enthalpy	Co	Fe	Mn	Ni
Cr	−4	−1	2	−7
Co		−1	−5	0
Fe			0	−2
Mn				−8

Table 3
SRO parameter for each atomic pair in the CoCrFeMnNi HEA averaged over thte last MC steps at 500 and 1200 K.

Pair	500K	1200K
Mn-Mn	0.067	0.0
Mn-Ni	0.067	−0.0833
Mn-Co	−0.083	0.0333
Mn-Cr	−0.050	−0.0167
Mn-Fe	0.0	0.0667
Ni-Ni	0.133	0.0
Ni-Co	0.0	0.1500
Ni-Cr	−0.183	0.0
Ni-Fe	−0.017	−0.0667
Co-Co	0.20	0.0
Co-Cr	−0.033	−0.1167
Co-Fe	−0.083	−0.0667
Cr-Cr	0.267	0.1667
Cr-Fe	0.0	−0.0333
Fe-Fe	0.10	0.10

Table 4
Electronegativity [28] and WS radii of Cr, Co, Fe, Mn, and Ni in a pure metal system and CrCoFeMnNi HEA, respectively.

Element	Electronegativity	WS radius in pure metal (Å)	WS radius in HEA (Å)
Cr	1.56	1.42	1.36
Co	1.70	1.38	1.39
Fe	1.64	1.41	1.38
Mn	1.60	1.52	1.38
Ni	1.75	1.37	1.39

reduced the total energy by 41 meV per atom compared to that of the SQS structure, indicating that it was more favorable for the CoCrFeMnNi HEA.

The existence of the SRO decreased the free energy due to a considerable devaluation of the mixing enthalpy through the transformation of the atomic pairing probabilities [23]. The mixing enthalpies of the binary systems containing the elements in CrCoFeMnNi HEA are listed in Table 2. A negative and a positive mixing enthalpy indicate that the binding atomic pairs decreases and increases the mixing enthalpy of the alloy system, respectively [25]. It was noted that approximately all the values of the mixing enthalpies were negative or close to zero, except for the Mn-Cr atomic pair. This was consistent with our prediction of the change in the atomic pairing possibilities, that is, the occurrence of SRO. At 500K, the major deviations from the fully random state were demonstrated in the accumulation of Ni-Cr and depletion of Cr-Cr pairs, as shown in Fig. 5 (b) and Table 3. The average number of Ni-Cr pairs increased to 2.8 from the fully random state of 2.4, and the number of Cr-Cr pairs decreased to 1.8. The enrichment of Ni-Cr accounted for the more negative mixing enthalpy between Cr and Ni. The depletion of Cr-Cr can potentially be related to the strong Cr-Cr repulsion due to the magnetic frustration originating from the nearest neighboring Cr-Cr, which was forced to align ferromagnetically [26]. A further investigation of Cr-Cr locations for the second and third shells revealed that a number of Cr atoms were located in the second shell, indicating a tendency of the formation of simple cubic Cr sublattice. Additionally, the same-type neighbors, including the Ni-Ni, Co-Co, Fe-Fe, and Mn-Mn pairs, were all depleted. Nevertheless, some other atom pairs exhibited local order, which had been predicated in detail in our simulations. The absolute value of SRO for each atomic pair was small, implying little local order (less than the resolution of the CDB method), but the overall alloy environment was disordered. Moreover, the configurational entropy term became more prominent at high temperatures, which can balance the effect of the mixing enthalpy to further reduce the local ordering [27]. The SRO parameter for each atom pair was zero at 1200 K, indicating a more disordered atomic arrangement with increasing temperature. Therefore, the calculated results of disordered element distribution in the CoCrFeMnNi HEA were in agreement with the experimental results.

On the other hand, the atomic size mismatch can cause serious lattice distortion and lower the phase transformation rate, which may lead to the segregation of atoms in the solid solution. Based on Eq. (2) and the WS radius of pure metals (as listed in Table 4), the atomic size mismatch was calculated to be 3.7%. However, in the alloying process of multiple elements, the electronegativity difference in each atom allows the transfer of electrons to reduce the total energy of the lattice structure and altered the atomic size of each atom. In the CrCoFeMnNi HEA, the electronegativity of each constituent element (see Table 4) was correlated with the *d*-electrons. As shown in Fig. 6, we demonstrated the charge difference of the *d*-orbitals exhibits a near linear dependence on the atomic size of each atom. The small (large) atoms tended to attract (ditch) electrons to decrease the atomic size difference. This tendency was consistent with the electronegativity difference between the two elements. Using the average WS radii of each elements in the CrCoFeMnNi HEA system (see the fourth column of Table 4), the value of the atomic size mismatch (δ) was reduced to 0.9%, which suggested that the charge transfer effect can mitigate the size mismatch and stabilize the solid solution.

Therefore, it was shown from the results of the experiments and simulation calculations that the segregation of the elements did not occur in the well-annealed CoCrFeMnNi HEA. Unfortunately, the hybrid MMC/DFT method cannot be applied to the simulation of the segregation of the CoCrFeMnNi HEA under irradiation, that is, in the state of nonequilibrium solid solution. Moreover, the introduction of defects

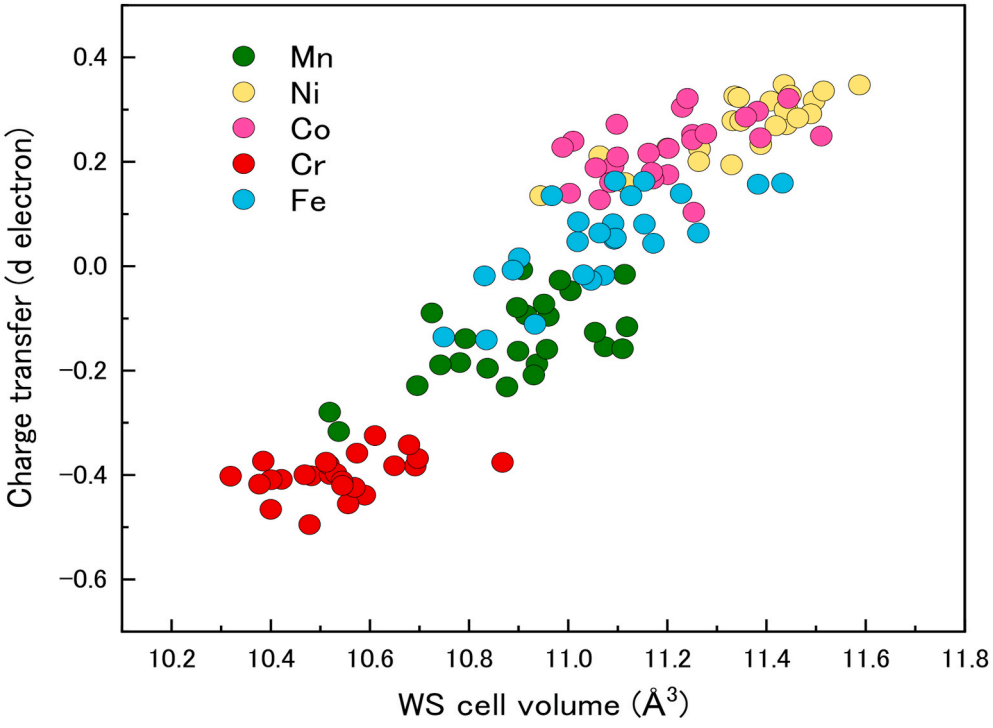

Fig. 6. Relationship between the charge transfer of *d*-orbitals on the Wigner–Seitz (WS) cell volume for each alloying atom in the CrCoFeMnNi HEA.

using irradiation raised the Gibbs free energy, which may cause segregation in the CoCrFeMnNi HEA [29]. As shown in Fig. 4, there was no segregation in the CoCrFeMnNi HEA after irradiation at 300, 573, and 773 K. Generally, the migration of point defects, such as the interstitials and vacancies, becomes faster with increasing temperature. Therefore, the diffusion of elements based on the vacancy mechanism was easier with increasing temperature. It was considered that the irradiation at 300 and 573 K was less likely to cause segregation in the CoCrFeMnNi HEA than that at 773 K. In addition, the irradiation at 773 K left fewer defect clusters, indicating that the CoCrFeMnNi HEA was resistant to irradiation [11]. Data so far are insufficient to fully explain the irradiation behavior of material. Further studies are needed to clarify the mechanism of the microstructural evolution of the CoCrFeMnNi HEA during irradiation.

4. Conclusion

The element distribution randomness of the CoCrFeMnNi equiatomic HEA was investigated using the positron annihilation spectroscopy and first-principles calculations. The experimental results showed that the well-annealed CoCrFeMnNi HEA had no significant element segregation. On the other hand, the calculation results showed the accumulation of Ni-Cr pairs as well as the depletion of same-type neighbors, especially Cr-Cr pairs, at 500 K; however, it was found that the atomic arrangement was random at 1200 K. The experimental and calculation results were consistent. Furthermore, the experimental results showed that there was no significant element segregation in the CoCrFeMnNi HEA irradiated by ions at 300, 573, and 773 K. It was found that the CoCrFeMnNi HEA had good irradiation resistance under these conditions.

CRediT authorship contribution statement

X.L. Ren: Data curation, Writing - original draft, Writing - review & editing, and Writing. **B.D. Yao:** Data curation. **T. Zhu:** Data curation. **Z. H. Zhong:** Investigation, Data curation. **Y.X. Wang:** Formal analysis. **X. Z. Cao:** Formal analysis. **S. Jinno:** Data curation. **Q. Xu:** Supervision, and, Conceptualization, Conceptualization.

Declaration of competing interest

The authors declare that they have no known competing financial interests or personal relationships that could have appeared to influence the work reported in this paper.

Acknowledgements

X.R. and Y.W. received financial support from the National Natural Science Foundation of China under Grant No. 11775051.

References

[1] J.W. Yeh, Alloy design strategies and future trends in high-entropy alloys, JOM 65 (2013) 1759–1771.
[2] Y. Zhang, T.T. Zuo, Z. Tang, M.C. Gao, K.A. Dahmen, P.K. Liaw, Z.P. Lu, Microstructures and properties of high-entropy alloys, Prog. Mater. Sci. 61 (2014) 1–93.
[3] B.S. Murty, J.W. Yeh, S. Ranganathan, High-Entropy Alloys, Butterworth-Heinemann, Elsevier, 2014.
[4] J.W. Yeh, S.K. Chen, S.J. Lin, J.Y. Gan, T.S. Chin, T.T. Shun, C.H. Tsau, S.Y. Chang, Nanostructured high-entropy alloys with multiple principal elements: novel alloy design concepts and outcomes, Adv. Eng. Mater. 6 (2004) 299–303.
[5] D.B. Miracle, J.D. Miller, O.N. Senkov, C. Woodward, M.D. Uchic, J. Tiley, Exploration and development of high entropy alloys for structural applications, Entropy 16 (2014) 494–525.
[6] M.H. Tsai, J.W. Yeh, High-entropy alloys: a critical review, Mater. Res. Lett. 2 (2014) 107–123.
[7] B. Cantor, I.T.H. Chang, P. Knight, A.J.B. Vincent, Microstructural development in equiatomic multicomponent alloys, Mater. Sci. Eng., A 375–377 (2004) 213–218.
[8] B. Gludovatz, E.P. George, R.O. Ritchie, Processing, microstructure and mechanical properties of the CrMnFeCoNi high-entropy alloy, JOM 67 (2015) 2262–2270.
[9] E.J. Pickering, N.G. Jones, High-entropy alloys: a critical assessment of their founding principles and future prospects, Int. Mater. Rev. 61 (2016) 183–202.
[10] A. Gali, E.P. George, Tensile properties oh high- and medium-entropy alloys, Intermetallics 39 (2013) 74–78.
[11] K. Jin, C. Lu, L.M. Wang, J. Qu, W.J. Weber, Y. Zhang, H. Bei, Effects of compositional complexity on the ion-irradiation induced swelling and hardening in Ni-Containing equiatomic alloys, Scripta Mater. 119 (2016) 65–70.
[12] Q. Xu, Z.H. Zhong, T. Zhu, X.Z. Cao, H. Tsuchida, Migration behavior of vacancies and damage structure recovery in a Fe-based FeCrMnCuMo multi-component alloy, Phil. Mag. 100 (2020) 1733–1748.
[13] B. Schuh, F. Mendez-Martin, B. Volker, E.P. George, H. Clemens, R. Pippan, A. Hohenwarter, Mechanical properties, microstructure and thermal stability of a nanocrystalline CoCrFeMnNi high-entropy alloy after severe plastic deformation, Acta Mater. 96 (2015) 258–268.
[14] W. Zhou, L.M. Fu, P. Liu, X.D. Xu, B. Chen, G.Z. Zhu, X.D. Wang, A.D. Shan, M. W. Chen, Deformation stimulated precipitation of a single-phase CoCrFeMnNi high entropy alloy, Interetallics 85 (2017) 90–97.
[15] A.F. Makhov, The penetration of electrons into solids. 2. The distribution of electrons in depth, Sov. Phys. Solid State 2 (1961) 1942–1944.
[16] A. Vehanen, K. Saarinen, P. Hautojarvi, H. Huomo, Profiling multilayer structures with monoenergetic positrons, Phys. Rev. B 35 (1978) 4606–4609.
[17] X.L. Ren, P.H. Shi, W.W. Zhang, X.Y. Wu, Q. Xu, Y.X. Wang, Swamps of hydrogen in equiatomic FeCuCrMnMo alloys: first-principles calculations, Acta Mater. 180 (2019) 189–198.
[18] J.M. Cowley, An approximate theory of order in alloys, Phys. Rev. 77 (1950) 669–675.
[19] X. Yang, Y. Zhang, Prediction of high-entropy stabilized solid-solution in multi-component alloys, Mater. Chem. Phys. 132 (2012) 233–238.
[20] M. Elsayed, R. Krause-Rehberg, C. Eisenschmidt, N. Eibmann, B. Kieback, Defect study in CoCrFeMnNi high entropy alloy by positron annihilation lifetime spectroscopy, Phys. Status Solidi 215 (2018), 1800036.
[21] Y. Nagai, M. Hasegawa, Z. Tang, A. Hempel, K. Yubuta, T. Shimamura, Positron confinement in ultrafine embedded particles: quantum-dot-like state in an Fe-Cu alloy, Phys. Rev. B 61 (2000) 6574–6578.
[22] N.L. Okamoto, K. Yuge, K. Tannaka, H. Inui, E.P. George, Atomic displacement in the CrMnFeCoNi High-entropy alloy - a scaling factor to predict solid solution strengthening, AIP Adv. 6 (2016), 125008.
[23] D.M. King, S.C. Middleburgh, L. Edwards, G.R. Lumpkin, M. Cortie, Predicting the crystal structure and phase transitions in high-entropy, alloys, JOM 67 (2015) 2375–2380.
[24] A. Takeuchi, A. Inoue, Classification of bulk metallic glasses by atomic size difference, heat of mixing and period of constituent elements and its application to characterization of the main alloying element, Mater. Trans. 46 (12) (2005) 2817–2829.
[25] A. Takeuchi, A. Inoue, Calculations of mixing enthalpy and mismatch entropy for ternary amorphous alloys, Mater. Trans. 41 (11) (2000) 1372–1378.
[26] A. Caro, M. Caro, P. Klaver, B. Sadigh, The computational modeling of alloys at the atomic scale: from ab initio and thermodynamics to radiation-induced heterogeneous precipitation, JOM 59 (2007) 52–57.
[27] D.J.M. King, S.C. Middleburgh, A.G. MvGregor, M.B. Cortie, Predicting the formation and stability of single phase high-entropy alloys, Acta Mater. 104 (2016) 172–179.
[28] E.J. Little, M.M. Jones, A complete table of electronegativities, J. Chem. Educ. 37 (5) (1960) 231–233.
[29] S.C. Middleburgh, D.M. King, G.R. Lumpkin, M. Cortie, L. Edwards, Segregation and migration of species in the CrCoFeNi high entropy alloy, J. Alloys Compd. 599 (2014) 179–182.